

Chemical Science

Accepted Manuscript



This is an *Accepted Manuscript*, which has been through the Royal Society of Chemistry peer review process and has been accepted for publication.

Accepted Manuscripts are published online shortly after acceptance, before technical editing, formatting and proof reading. Using this free service, authors can make their results available to the community, in citable form, before we publish the edited article. We will replace this *Accepted Manuscript* with the edited and formatted *Advance Article* as soon as it is available.

You can find more information about *Accepted Manuscripts* in the [Information for Authors](#).

Please note that technical editing may introduce minor changes to the text and/or graphics, which may alter content. The journal's standard [Terms & Conditions](#) and the [Ethical guidelines](#) still apply. In no event shall the Royal Society of Chemistry be held responsible for any errors or omissions in this *Accepted Manuscript* or any consequences arising from the use of any information it contains.



Journal Name

ARTICLE

When the Inhibitor Tells More than the Substrate: the Cyanide-Bound State of a Carbon Monoxide Dehydrogenase

Alexandre Ciaccafava,^{a†*} Daria Tombolelli,^{a†} Lilith Domnik,^b Jochen Fessler,^b Jae-Hun Jeoung,^b Holger Dobbek,^b Maria Andrea Mroginski,^{a*} Ingo Zebger,^{a*} Peter Hildebrandt^a

Received 00th January 20xx,
Accepted 00th January 20xx

DOI: 10.1039/x0xx00000x

www.rsc.org/

The Carbon Monoxide Dehydrogenase (CODH) is a key enzyme for reversible CO interconversion. To elucidate structural and mechanistic details of CO binding at the CODH active site (C-cluster), cyanide is frequently used as an iso-electronic substitute and inhibitor. However, previous studies revealed conflicting results on the structure of the cyanide-bound complex and the mechanism of cyanide-inhibition. To address this issue in this work, we have employed IR spectroscopy, crystallography, site directed mutagenesis, and theoretical methods to analyse the cyanide complex of the CODH from *Carboxydotherrmus hydrogenoformans* (CODH_{II_{Ch}). IR spectroscopy demonstrates that a single cyanide binds to the Ni ion. Whereas the inhibitor could be partially removed at elevated temperature, irreversible degradation of the C-cluster occurred in presence of excess cyanide on the long-minute time scale, eventually leading to the formation of [Fe(CN)₆]⁴⁻ and [Ni(CN)₄]²⁻ complexes. Theoretical calculations based on a new high resolution structure of the cyanide-bound CODH_{II_{Ch} indicated that cyanide binding to the Ni ion occurs upon dissociation of the hydroxyl ligand from the Fe₁ subsite of the C-cluster. The hydroxyl group is presumably protonated by Lys563 which, unlike to His93, does not form a hydrogen bond with the cyanide ligand. A stable deprotonated ε-amino group of Lys563 in the cyanide complex is consistent with the nearly unchanged C≡N stretching in the Lys563Ala variant of CODH_{II_{Ch}. These findings support the view that the proton channel connecting the solution phase with the active site displays a strict directionality, controlled by the oxidation state of the C-cluster.}}}

Introduction

The O₂-sensitive [Ni-Fe] Carbon Monoxide Dehydrogenase (CODH) is a homodimeric enzyme responsible for the biological interconversion between CO and CO₂ according to the reaction: CO+H₂O ↔ CO₂+2H⁺+2e⁻. CODHs play crucial roles in various metabolic pathways, including the Wood-Ljungdahl pathway that allows anaerobic microorganisms, such as acetogenic firmicutes *Moorella thermoacetica* (*Mt*) and hydrogenogenic firmicutes *Carboxydotherrmus hydrogenoformans* (*Ch*) to grow on H₂ and CO₂ as electron and carbon source, or to oxidise CO using it as source of electrons¹.

The CODH hosts a unique [NiFe₄S₄OHx] cluster, called C-cluster, which efficiently catalyses the reversible CO oxidation reaction². Briefly, the C-Cluster resembles a classical cubane shape [4Fe-4S] from which one Fe is pulled out and left to

dangle. The dangling Fe, so called Fe₁, presumably binds a hydroxyl ligand while the vacant Fe position has been filled by a Ni atom. The C-cluster adopts at least two different oxidation states during catalysis. The C_{red1} redox state is able to bind CO while C_{red2}, obtained by a further, two-electron reduction, specifically targets CO₂. The midpoint potential of C_{red1}/C_{red2} couple (-530 mV vs SHE) almost matches the midpoint potential of the substrates (E⁰ CO/CO₂ = -558 mV, pH 7)³. Moreover, turnover frequencies up to 40000 s⁻¹ and Michaelis constants of ~ 20 μM have been reported for CO oxidation by two CODHs from thermophilic bacteria *Ch* and whereas the corresponding values for CO₂ reduction by the CODH of *Rhodospirillum rubrum* were found to be ca. 45 s⁻¹ and 200 μM, respectively⁴⁻⁵.

Important information about the catalytic cycle was obtained by X-ray crystallography^{2, 6-8}. Particularly, the recent atomic-resolution structures of CODH_{II_{Ch} (d_{min} ≤ 1.1 Å) provided insight into binding and activation of CO₂ (and its inhibitory counterpart NCO)⁹. Notably, both CO₂ and NCO had undergone a two-electrons reduction step and the respective products were stabilised via π-backbonding. Such a detailed picture is yet not available for CO binding to the C-cluster, although structural analysis pointed to a bent geometry of CO (or formyl) bound to the terminal Ni in the CODH-CO complex}

^a Technische Universität Berlin, Institut für Chemie, Sekretariat PC 14, D-10623 Berlin, Germany. E-mails: alex.ciacca@gmail.com, andrea.mroginski@tu-berlin.de, ingo.zebger@tu-berlin.de

^b Humboldt-Universität zu Berlin, Institut für Biologie, Unter den Linden 6, D-10099 Berlin, Germany.

† These authors contributed equally.

Electronic Supplementary Information (ESI) available: Table S1. Statistics on Data collection and structure refinement. See DOI: 10.1039/x0xx00000x

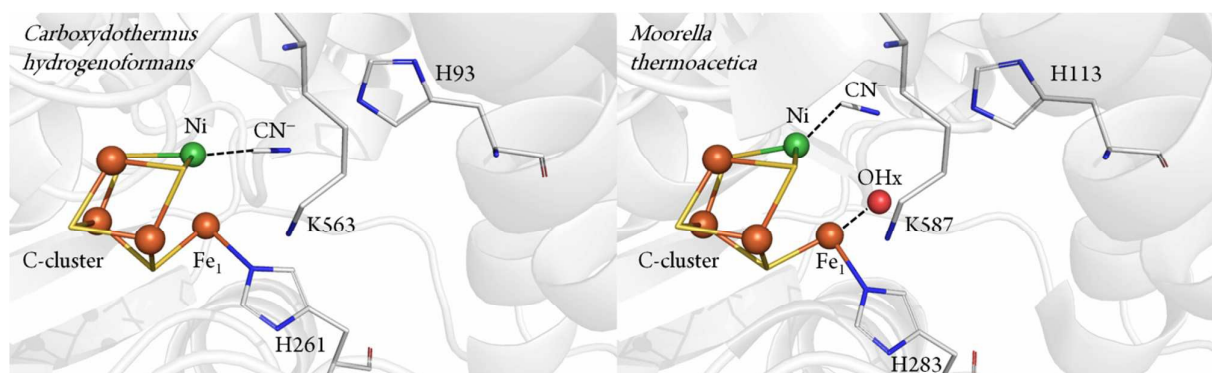


Fig.1: Comparison between CN^- bound C-Cluster of CODHII_{ch} (pdb:3I39) and CODHIII_{ch} (pdb:3I04), according to references^{7,8}.

of *Methanosarcina barkeri*¹⁰. This finding was consistent with the view that a bent Ni-CO geometry would lower the energetic activation barrier for CO oxidation. In a complementary crystallographic study, cyanide (CN^-), a structural analogue of CO and inhibitor of CODH, was found to possess a similar bent conformation⁷. Recently, however, an independent re-evaluation of the electron density maps of these two structures (resolution $\geq 2\text{\AA}$) did not provide clear evidence for the orientation of the CO or the CN^- ligand¹¹. In addition, another crystal structure presenting a different binding mode of CN^- has been reported for CODHII_{ch} ⁸ (Fig.1).

In principle, spectroscopic techniques such as IR spectroscopy may contribute to rationalise these partially conflicting results. In particular, IR spectroscopy is an ideal tool since it probes the $\text{C}\equiv\text{N}$ stretching mode in a spectral region free of any interfering bands of the protein. However, the results reported in previous IR spectroscopic studies on *Clostridium thermoaceticum* CODH (CODH_{ct}) revealed multiple signals in the $\text{C}\equiv\text{N}$ stretching region¹²⁻¹³ that cannot readily be reconciled with the current structural data. In this work, we have therefore set up an integral approach including IR spectroscopic, crystallographic, site directed mutagenesis and theoretical analysis. Spectroscopic measurements were carried out with the wild-type and engineered CODHII_{ch} variant to assess the parameters that control the $\text{C}\equiv\text{N}$ stretching frequency. This analysis served as a reference for the quantum-mechanical / molecular mechanics (QM/MM) calculations which were performed on the basis of new high-resolution crystal structures to elucidate details of the active site structure of the CODHII_{ch} -CN complex.

Material and methods

Sample preparation:

Buffers and reagents were anoxically prepared in a glovebox. Inhibition procedures described below are performed under the same anoxic conditions. In addition to the inherent safety risks while handling cyanide, it is worth noticing that controlling precisely cyanide concentration is not straightforward, especially when using buffer in the

physiological relevant range, *i.e.* pH 7-8, as the pK_a value for HCN is 9.21. Therefore, the band position of the $\text{C}\equiv\text{N}$ stretching mode ranges from 2080 cm^{-1} (aqueous CN^-) to 2093 cm^{-1} (dissolved HCN), when the pH is decreased below the pK_a . This is the pH range, where the enzyme exhibits its highest activity. Thus, the absolute concentration effect of CN^- has to be estimated with caution. Protein expression and purification were performed as described earlier². Protocol A: 6 μL of CODHII_{ch} 400 μM were diluted in 500 μL of buffer A (Tris-HCl 50 mM pH 8, NaCl 100 mM) containing either dithionite (DT) 4 mM or Titanium citrate (Ti(III) citrate) 5 mM and incubated for 45 minutes. Cyanide (1 mM) was added to the sample and allowed to react with CODHII_{ch} for 30 minutes under gentle stirring. The CODHII_{ch} sample was subsequently washed several times using Microcon® Centrifugal Filters (cut-off 100kDa) with buffer A and reductant in order to remove excess cyanide and finally concentrated to 10 μL prior to injection into the transmission cell. Protocol B: 6 μL of CODHII_{ch} 400 μM were added to 6 μL of an inhibition mixture containing cyanide (ranging from 2 to 20 mM) and DT (4 mM) in buffer A. Finally, 10–12 μL of the inhibited CODHII_{ch} sample which was prepared according to procedures described above was injected into a gas-tight transmission cell. Protocol C: Crystals of CODHII_{ch} were incubated in buffer A' (25 % PEG3350, 50 mM Tris-HCl pH 8.0 and 5 mM Ti(III) citrate or DT 4 mM). Crystals were then transferred into a buffer B solution containing (25 % PEG3350, 50 mM Tris-HCl pH 8.0, 7 mM DTT), and 0.5 mM of oxidised methylviologen (MV_{ox}) as electron acceptor for reoxidation. After no further reduction of MV_{ox} to the blue colored reduced methylviologen (MV_{red}) was detectable, the crystals were incubated in buffer B solution containing 7 mM DTT for 2 hours. Finally, crystals were transferred into a buffer B solution containing 5 mM KCN and loaded into the transmission cell.

Enzymatic assays:

Inhibited aliquots of CODHII_{ch} were reactivated under CO atmosphere at 70°C for 30 min. Then the CO oxidation activity was assayed as described before⁴.

Fourier Transform Infrared Spectroscopy:

FTIR spectra were recorded on a Bruker Tensor 27 spectrometer equipped with a liquid nitrogen-cooled MCT detector applying a spectral resolution of 2 cm^{-1} . The sample compartment was purged with dried air, and the sample was held in a temperature-controlled ($10\text{ }^\circ\text{C}$) gas-tight IR-cell for liquid samples (volume $\sim 10\text{ }\mu\text{L}$, path length = $50\text{ }\mu\text{m}$) with CaF_2 windows. Spectra were base-line corrected by using the OPUS software from Bruker.

Crystallization and manipulation of crystals:

CODHII_{Ch} crystals and the -320 mV state were produced as described earlier^{2, 8}. Crystals in the -320 mV state were incubated with 70 mM KCN for 30 min . CN^- -soaked crystals were shock-frozen in liquid nitrogen, generating the $-320\text{ mV CODHII}_{Ch}\text{-CN}$ state, with 15% (v/v) $2R, 3R$ -butanediol (Sigma) serving as cryoprotectant.

Data collection, structure solution and refinement:

Diffraction data were collected at 100 K at a wavelength of 0.9184 \AA at BESSY II (Berlin, Germany)¹⁴. The synchrotron data set was integrated and scaled using XDSAPP¹⁵. Data statistics are reported in Table S1 (see supporting information). Initial rigid body refinement was used to solve phasing, followed by a simulated annealing refinement to minimise model bias using PHENIX¹⁶. Models were built and refined with COOT¹⁷. Positional and temperature factor refinements were carried out using Refmac5¹⁸⁻¹⁹. New parameters for the C-cluster were generated by iterative cycles of refinement using Refmac5. Individual occupancies of atoms from the C-cluster were adjusted until comparable B factors of atoms were obtained. In the final refinement cycles the B factors were refined anisotropically and alternative conformations of several side chains and Fe_1 were included. The final refinement statistics are shown in Table S1 of ESI. The atomic coordinates have been deposited in the Protein Data Bank, www.pdb.org (PDB ID: 5FLE)

Theoretical methods:

The eight structural models listed in Table 2, were built starting from two crystal structures of the CODHII_{Ch} in the -320mV state. The first one, with pdb: 5FLE, represents the CN^- bound state refined in this work, while the second structure is inhibitor free (pdb: 3B53). In the latter one, a starting geometry for the CN^- bound state was generated by attaching a CN^- ligand to the Ni atom. The protein was solvated in an explicit TIP3P water box of dimension $130 \times 130 \times 130\text{ \AA}^3$. Hydrogens were inserted and protonable side chains were set to their standard states at pH 7. Protonation states of some specific residues, e.g. those in the vicinity of the C-cluster or involved in suggested proton transfer pathways, required special attention based on chemical sense and visual inspection²⁰. Although the His93 was doubly protonated on N δ and on N ϵ , further investigation was required to test different protonation states of this residue together with Lys563, since they are interacting via hydrogen bonds with the non-proteic ligands at the active site. First, 20000 steps of energy minimization were performed using NAMD²¹ with the

CHARMM22 force field²². Hydrogen positions and orientation of water molecules were optimised. Heavy atoms were kept fixed to their initial positions, in order to obtain a good starting point for the subsequent geometry optimization and, at the same time, to remain as close as possible to the crystal structure conformation. Due to the lack of specific force field parameters, the five metal clusters (three standard $[\text{4Fe-4S}]$ and two $[\text{NiFe}_3\text{S}_4\text{-Fe}]$) were initially kept fixed during the energy minimization steps. Charges for the metal clusters were computed with DFT methods while Van der Waals parameters were taken from values reported for similar systems in the literature²³. The structure resulting from the last minimization step was then refined through hybrid QM/MM calculations, performed within the ChemShell environment²⁴. The program interfaces to a variety of QM and MM codes. In our work, Turbomole was chosen as the quantum chemical program while the MM uses DL_POLY with CHARMM22 force field. The system was divided in three layers, each of which treated at a different level of theory and accuracy. The QM part consists of (1) the $[\text{NiFe}_3\text{S}_4]$ C-cluster and the iron Fe_1 ; (2) Cys295, Cys333, Cys446, Cys476 and Cys526, which coordinate the Fe atoms of the cluster; (3) His261, which is interacting with Fe_1 ; (4) all the other non-proteic ligands that includes cyanide on Ni in different positions and hydroxyl on Fe_1 in some of the models; (5) His93, Lys563 interacting directly with the non-proteic ligands, Gln332 interacting via hydrogen bond with Lys563 and Ile567 whose role is important regarding the steric hindrance exerted on the cyanide ligand. DFT was employed in the optimization of the QM part, applying the pure density functional BP86 combined with the resolution-of-the-identity ('RI') technique²⁵. The def2-TZVP basis set was used for metals (Ni and Fe), while the 6-31G* basis set was employed for all other atoms of the QM part. This combination of a high quality basis set and BP86 functional is able to give both accurate molecular structures and harmonic vibrational frequencies, due to an error compensation that allows direct comparison of calculated harmonic frequencies with experimental ones²⁶. The second layer was made up of protein residues and water molecules included in a sphere of 15 \AA around the Ni atom of the C-cluster in monomer A. All the atoms in this section were treated in an explicit manner at the MM level and allowed to move during the optimization cycles. For this purpose the HDLC optimiser was employed²⁷. The third layer includes the remaining atoms not included in the previous two. This layer was held fixed during the QM/MM geometry optimization. Covalent bonds at the QM/MM border were cut and saturated by hydrogen link atoms. The coupling between QM and MM was computed using electrostatic embedding with a charge-shift scheme²⁴. Once optimised, the structures were analysed and compared with the crystal structure. The latter was based on some fundamental geometrical parameters like bond lengths and bond angles. In addition, a tilt angle was defined as the angle between a unit vector with origin in the center of the plane formed by Ni-S- Fe_4 -S and a unit vector directed along the Ni-CN bond axis.

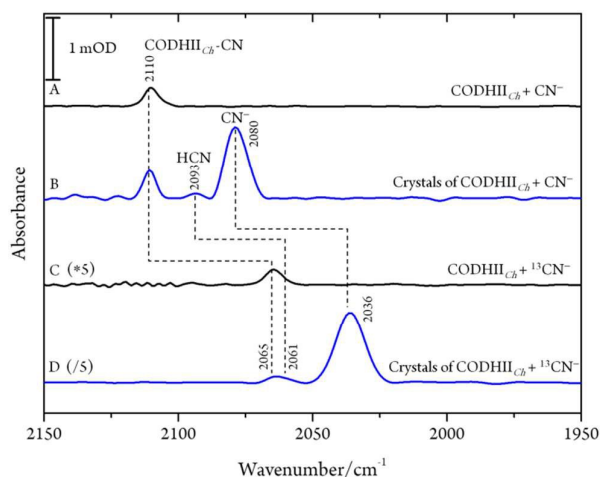


Fig.2: IR spectra of the CODHII_{Cb}-CN complex at pH8, 10°C. A, CODHII_{Cb} in solution after 30 min of exposure to CN⁻; B, crystalline state of CODHII_{Cb} after treatment with CN⁻; C, CODHII_{Cb} in solution after 30 min of exposure to ¹³CN⁻; D, crystalline state of CODHII_{Cb} after treatment with ¹³CN⁻.

Finally the vibrational frequencies of the quantum mechanical part in the optimised conformation were computed in presence of the point charges of the surrounding atoms of the second and third layers. For this purpose the Gaussian09 program was used with the same DFT functional and basis set employed during the optimization²⁸.

Results

IR spectroscopic identification of the CN⁻ inhibited state:

After exposure of CODHII_{Cb} to CN⁻ according to protocol A (see materials and methods), a sharp band immediately appears in the C≡N stretching region at 2110 cm⁻¹ (Fig.2A). The frequency upshift with respect to the free CN⁻ anion (2080 cm⁻¹) is expected since Ni is a weak π-donor metal²⁹. Band position and intensity are stable for hours. The frequency at 2110 cm⁻¹ is significantly higher than for cyanide bound Fe²⁺ heme proteins such as Horseradish peroxidase, microperoxidase and myoglobin (between 2029 cm⁻¹ and 2057 cm⁻¹), illustrating the rule of electronegativity (Ni>Fe) discussed previously³⁰⁻³¹. The origin of the band was further proven with labelled ¹³CN⁻ (2065 cm⁻¹), revealing the expected isotopic shift of 45 cm⁻¹ (Fig. 2C).

Next, we studied the CODHII_{Cb}-CN complex in the crystalline state which was prepared following the same protocol as used for crystallographic analysis. Several of these crystals were loaded into an IR transmission cell (Fig.2B and D). The IR spectra obtained in this way revealed a band at 2110 cm⁻¹ that shifts down by 45 cm⁻¹ to 2065 cm⁻¹ when crystals were incubated with ¹³CN⁻. Thus, the frequency (and isotopic shift) of the Ni-bound cyanide of the crystalline complex is the same as for the sample in solution.

Reversibility of CN⁻ binding:

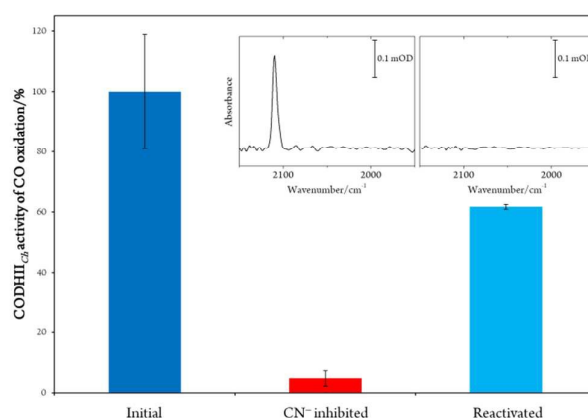


Fig.3: Plot representing the percentage of CO oxidation activity by CODHII_{Cb} before inhibition (blue column), after inhibition (red column) and after reactivation (light blue column). Inset: IR spectra of the inhibited CODHII_{Cb} before and after reactivation.

In order to prove the reversibility of the inhibition process³², we prepared a batch of inhibited CODHII_{Cb} that we used in parallel for enzymatic activity assay and IR spectroscopy. A classical enzymatic assay for CO oxidation by CODHII_{Cb} based on reduction of methylviologen was performed to evaluate the initial enzymatic activity (see materials and methods). Subsequently, the enzyme was inhibited following protocol A, and afterwards a new enzymatic assay for CO oxidation was performed. The inhibited protein exhibited not more than 5% of the initial CO oxidation activity (Fig.3). In parallel the corresponding enzyme was also loaded into a transmission cell for IR measurement and revealed the characteristic C≡N stretching band at 2110 cm⁻¹ (Fig.3 inset). Finally, the enzyme was reactivated at 70°C under CO atmosphere for 30 minutes and tested for CO oxidation afterwards. More than 60% of CO oxidation was recovered thereby proving a high reversibility of the CN⁻ binding (Fig.3).

These results are, however, not in agreement with previous IR data published for CN⁻ inhibition of CODH_{Ct}¹²⁻¹³. These authors observed a band at 2037 cm⁻¹ (1995 cm⁻¹ with ¹³CN⁻) and a second absorption appearing only at higher CN⁻ concentration at 2079 cm⁻¹ (2037 cm⁻¹ with ¹³CN⁻). However, the preparation protocol employed in that work did not include the removal of excess cyanide. In fact, when we repeated the experiments upon omitting the final buffer exchange step (protocol B, see materials and methods) we observed several bands at 2124 cm⁻¹, 2093 cm⁻¹ and 2037 cm⁻¹ shifting to 2078 cm⁻¹, 2061 cm⁻¹ and 1995 cm⁻¹ upon exposure to ¹³CN⁻, respectively (Fig. 4A and B).

While the assignment of the band at 2093 cm⁻¹ and its isotopically 32 cm⁻¹ shifted counterpart at 2061 cm⁻¹ to HCN and H¹³CN is straightforward³³, the origin of the two other bands is less obvious. Since only one binding site for CN⁻ is available in CODHII_{Cb} structure⁸, the presence of two extra bands is surprising. Moreover, these two features appear with a very slow rising time (≥ 5 hours) (Fig.5). In contrast, formation kinetics of the cofactor-cyanide adduct according to protocol A (removal of excess cyanide) and reflected by the 2110 cm⁻¹ band is not resolved on the time scale of these

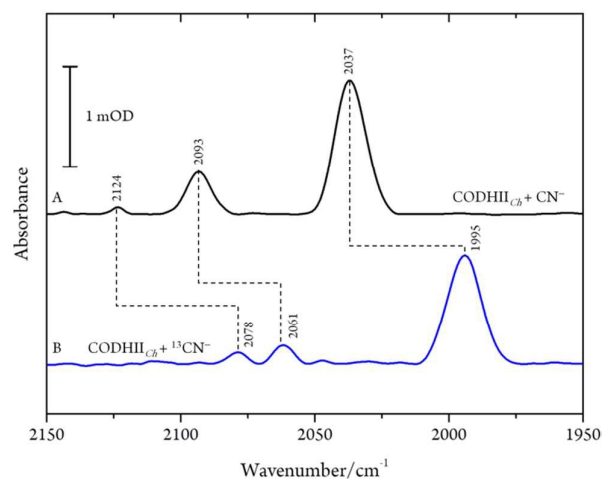


Fig.4: Infrared spectra of CODHII_{Ch} at pH8, 10°C left with A) CN⁻ and B) ¹³CN⁻ with a CN⁻/CODHII_{Ch} ratio of 100/1 measured at 10°C.

experiments and, hence, must occur on the minute time scale or faster (< 30 min), (Fig. 5).

CN⁻-induced degradation of the C-cluster:

Even though CN⁻ has been described as a slow reversible inhibitor, CODHII_{Ch} is fully inhibited in less than one minute at 70°C with 1 mM KCN under turnover conditions and in less than 80 min at 23°C with 0.1 mM KCN under non-turnover conditions as described in a previous study³². Furthermore, CN⁻ is known to have a high affinity towards metal ions including Fe and Ni which are the main components of the C-cluster, therefore, we suspected that prolonged exposure of CODHII_{Ch} to CN⁻ might lead to the formation of various cyano-metallic complexes. Therefore, we performed control experiments in order to verify the possible CN⁻ induced degradation of the metal clusters due to prolonged exposure of CODHII_{Ch} to CN⁻.

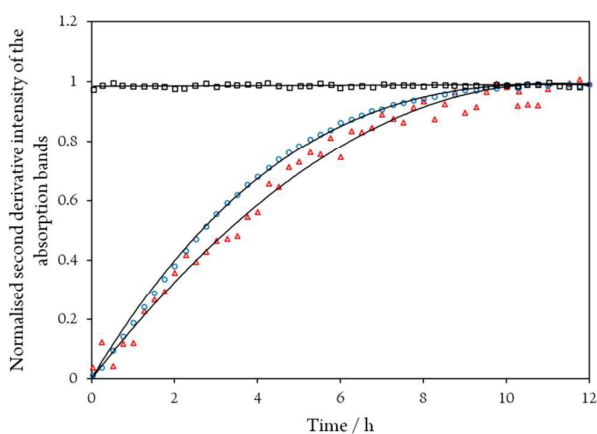


Fig.5: Time evolution of the normalised second derivative intensity of the absorption bands at 2110 cm⁻¹ for CODHII_{Ch} inhibited with CN⁻ according to protocol A (black square), and of the bands at 1995 cm⁻¹ (blue circles) and 2078 cm⁻¹ (red triangles) for CODHII_{Ch} inhibited with ¹³CN⁻ according to protocol B, respectively. Note that bands at 1995 cm⁻¹ and 2078 cm⁻¹ did not start at zero intensity and were normalised to one for better comparison.

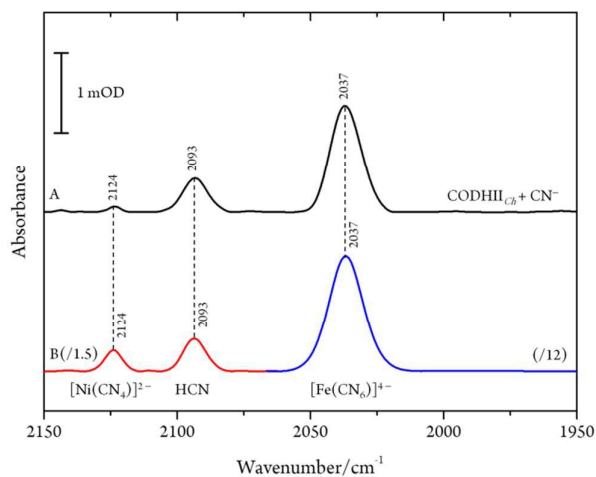


Fig.6: A) Infrared spectra of CODHII_{Ch} left with CN⁻ with a CN⁻/CODHII_{Ch} ratio of 100/1 and B) NiCl₂ 0.2 mM incubated with CN⁻ 1 mM (red line) and [Fe(CN)₆]⁴⁻ 1 mM (blue line) measured at 10°C, pH8. Spectra of cyano-metallic complexes are scaled down for better comparison.

The corresponding IR spectra were measured under the same experimental conditions as used for CODHII_{Ch} inhibition studies (Fig.6). Thus, nickel chloride (NiCl₂) has been incubated with CN⁻, resulting in the appearance of an absorption band at 2124 cm⁻¹ (2078 cm⁻¹ with ¹³CN⁻) (Fig.6B red line), which can be assigned to [Ni(CN)₄]²⁻ complex²⁹. In addition, the corresponding cyano complex of iron, [Fe(CN)₆]⁴⁻, exhibits an absorption band at 2037 cm⁻¹ (1995 cm⁻¹ for ¹³CN⁻) (Fig.6B blue line)^{30, 34-35}.

Accordingly, the control experiments allowed an assignment of the three bands observed for CODHII_{Ch} inhibition according to the alternative protocol B. Two of these bands, i.e. at 2080 cm⁻¹ (2036 cm⁻¹ for ¹³CN⁻) and 2037 cm⁻¹ (1995 cm⁻¹ for ¹³CN⁻) at pH8, are readily attributed to aqueous CN⁻ and [Fe(CN)₆]⁴⁻, respectively. The frequencies agree very well with those reported by Qiu *et al.* for CODH_{Ct} although the assignment suggested by these authors can be ruled out¹³. The third band at 2124 cm⁻¹ (2078 cm⁻¹ for ¹³CN⁻) was not reported by these authors although a weak band at *ca.* 2078 cm⁻¹ can be identified in the published spectrum of the CODH_{Ct} ¹³CN⁻ adduct in the corresponding figure. This band at 2124 cm⁻¹ band is now assigned to the C≡N stretching of [Ni(¹³CN)₄]²⁻ (Table 1).

Parameters controlling the C≡N stretching mode:

It was suggested previously that, depending on the concentration, cyanide may bind in different modes to the C-cluster³⁶. IR experiments were, therefore, carried out using different CN⁻/CODHII_{Ch} molar ratios from large excess (1000/1) to substoichiometric (1/2) amounts. These experiments did not reveal any additional band nor any frequency shifts of the only observed band at 2110 cm⁻¹ (data not shown). Furthermore, another, alternative binding mode was proposed to involve a hydroxyl ligand on the dangling Fe₁^{1, 36-37}, which should be sensitive to the local proton concentration. Thus, cyanide inhibition was studied as a function of the pH.

Table 1: C≡N stretching frequencies observed experimentally for CODHII_{Ch}-CN adducts according to protocol A and B. Control experiments and published data are also reported.

	Wavenumber / cm ⁻¹			
	Sample	$\nu(\text{CN})$	$\nu(^{13}\text{CN})$	$\Delta\nu(\text{CN} - ^{13}\text{CN})$
Controls	CN ⁻ (aq.)	2080	2036	44
	HCN (gas.)	2093	2061	32
	[Fe(CN) ₆] ⁴⁻	2037	1995	42
	[Ni(CN) ₄] ²⁻	2124	2078	46
Protocol A	CODHII _{Ch}	2110	2065	45
	CODHII _{Ch}	2037	1995	42
Protocol B	CODHII _{Ch}	2093	2061	32
	CODHII _{Ch}	2124	2078	46
	CODH _{Ct}	2079	2037	42
Published data	CODH _{Ct}	2037	1995	42

Data taken from literature are written in *italic*.

Whereas the C≡N frequency at 2110 cm⁻¹ remained unaffected in the pH range from 6 to 10, the related band intensities displayed a bell-like shape with a maximum at pH 8 (Fig.7). Again, these findings argue against any pH-dependent changes of ligand binding at the C-cluster. Instead, the intensity changes most likely reflect pH-dependent alterations of the active site accessibility for CN⁻.

There are also no qualitative changes of cyanide binding depending on the temperature.

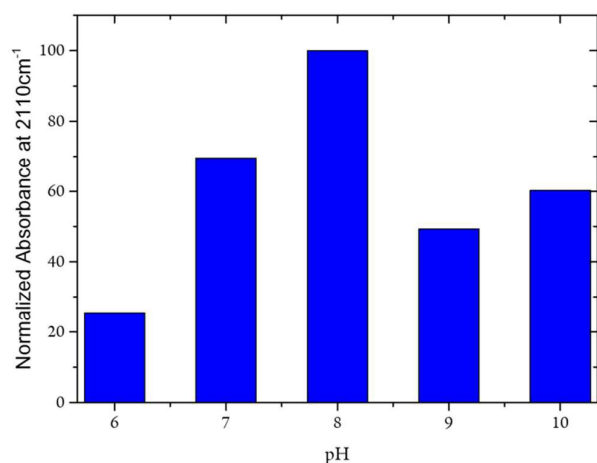


Fig.7: Intensity of the C≡N stretching mode at 2110 cm⁻¹ of the CODHII_{Ch}-CN adduct plotted as a function of the pH. Intensities were normalised with respect to the intensity of the corresponding amide II band.

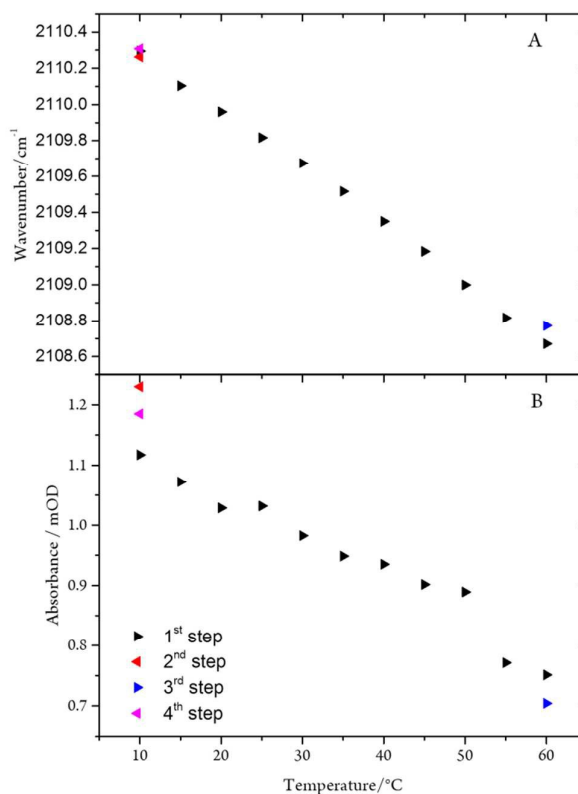


Fig.8: (A) Frequency and (B) intensity changes of the C≡N mode of the CODHII_{Ch}-CN adduct as a function of the temperature. The arrow tip points to the direction of the temperature steps.

The C≡N stretching frequency and the band intensity decrease only slightly (by 2.0 cm⁻¹ and ~30%, respectively) upon raising the temperature from 10°C to 60°C (Fig. 8). Conversely, in the frozen state (100 K) the frequency is increased by only 5 cm⁻¹. These spectral variations can be rationalised in terms of subtle conformational changes of the protein in the vicinity of the C-cluster. Consistent with this explanation is the observation that the temperature-dependent changes are fully reversible, underpinning the remarkable stability of the CODHII_{Ch}-CN adduct.

Environmental effects on the C≡N stretching mode:

According to X-ray data, Ni-bound cyanide is in close vicinity to His93 and Lys563 which may interact with the cyanide-bound metal center. We therefore extended the studies to the CODHII_{Ch} variant with alanine substitution at the corresponding position. Addition of cyanide to the Lys563A variant displayed a wild-type like IR spectrum since the $\nu(\text{C}\equiv\text{N})$ undergoes a downshift from 2110 to 2102 cm⁻¹.

Crystal structures of CN⁻-inhibited CODHII_{Ch}:

Table 2. Calculated and experimental structural and spectroscopic quantities of the C-cluster

Structures		Distances / Å				Angles / °		Presence of	$\nu(\text{CN}) / \text{cm}^{-1}$		
name	specificity origin	Ni-Fe ₁	Ni-C _{CN}	N _{CN} -N _{K563}	N _{CN} -N _{E93}	CN-tilt	Ni-C-N	OH ⁻	calc.	$\Delta(\text{exp.}-\text{calc.})$	
CODHII _{Ch} -CN <i>pdb(5FLE)</i>	- exp.	2.67	1.92	3.00	2.66	5.98	168	no	-	-	
	- calc.	2.65	1.81	2.98	2.72	6.40	169	no	2074	-36	
	/tilt calc.	2.66	1.82	3.79	2.69	18.42	171	no	2107	-3	
	/tilt/OH ⁻ calc.	2.94	1.85	4.59	2.82	29.07	165	yes	2054	-56	
	/K563dep. calc.	2.73	1.83	3.97	2.72	24.44	173	no	2109	-1	
	/K563A calc.	2.71	1.83	-	2.70	23.52	173	no	2112	+10	
CODHII _{Ch} -C _{red1} -CN* <i>pdb(3B53)</i>	- calc.	2.63	1.80	2.88	2.74	3.03	175	no	2058	-52	
	/tilt calc.	2.68	1.81	3.94	2.66	17.71	175	no	2129	+19	
*: CN ⁻ was added <i>in silico</i>		/tilt/OH ⁻ calc.	2.86	1.83	4.65	2.76	37.35	165	yes	2054	-56

Abbreviations used in Table.2: calc.: calculated, exp.: experimental, dep.: deprotonated. The corresponding structure names, in the text, are defined by assembling the column name and specificity.

We have determined a new crystal structure of CN⁻ bound CODHII_{Ch} (*pdb* 5FLE) at a resolution of 1.23 Å. As expected, the 2009 structure (*pdb*:3I39, *dmin*= 1.35 Å) and the new CODHII_{Ch}-CN structure are nearly identical with a rmsd for core C α atoms of 0.14 Å. The main difference between the two structures is the degree of multiple conformations. While the 2009 structure revealed dual conformations for residues starting from the Fe₁-coordinating His-261 down to residue 266 as well as residues in their vicinity, the electron density of these parts agree now with only a single conformation, indicating a more homogeneously CN⁻ bound state⁸.

QM/MM calculations:

Two different experimentally determined structures served as starting points for the QM/MM calculations. First, we used the crystal structure of the CODHII_{Ch}-CN inhibited state determined in this work (*pdb*: 5FLE). Geometry optimization did not affect the main structural parameters of the C-Cluster and residues surrounding the CN⁻ ligand except for Ni-C(CN) bond length, which was predicted to be shorter by 0.11 Å compared to the experimental value (Table 2). A comparably short Ni-C bond length was also reported in a previous QM/MM study by Amara *et al.*¹¹ and recently observed in CO₂ and NCO bound structures⁹. Also in the previous CODHII_{Ch}-CN structure, solved at lower resolution (1.35 Å), a shorter bond length was determined⁸, in line with the results of an earlier EXAFS study³². In agreement with the experimental structure, the calculations predict the Ni atom in a square planar geometry with a tilt angle of 6.40° of the CN⁻ ligand (See material and methods, section QM/MM for tilt angle definition). In this configuration, the CN⁻ ligand is in hydrogen

bonding distance to the side chains of His93 (2.72 Å) and Lys563 (2.98 Å).

Second, calculations were carried out starting with the CODHII_{Ch} structure of the -320 mV reduced state (*pdb*:3B53) to which we added a CN⁻ ligand *in silico* (CODHII_{Ch}-C_{red1}-CN). Prior to optimization, we have removed the water molecule in the vicinity of the CN⁻ binding site to keep in line with the experimental structure of CODHII_{Ch}-CN. Between both optimised structures a very good agreement was obtained with respect to the geometries of the C-cluster and CN⁻ environment (Table.2). Also for the optimised CODHII_{Ch}-C_{red1}-CN structure a small tilt angle (3.03 Å) for the CN⁻ ligand and similar distances to His93 (2.74 Å) and Lys563 (2.88 Å) were obtained.

The C≡N stretching frequencies were calculated to be 2074 cm⁻¹ and 2058 cm⁻¹ for CODHII_{Ch}-CN and CODHII_{Ch}-C_{red1}-CN, respectively. They are both significantly lower than the experimental value of 2110 cm⁻¹.

As postulated previously^{7, 36}, CN⁻ may initially bind to complete a distorted tetrahedral coordination geometry at the Ni. Thus, an alternative geometry optimization was started by setting the initial tilt angle to 60.71°. In fact, the subsequent energy minimization afforded different minima for both CODHII_{Ch}-CN (CODHII_{Ch}-CN/tilt) and CODHII_{Ch}-C_{red1}-CN (CODHII_{Ch}-C_{red1}-CN/tilt) with somewhat higher tilt angles of ~18°. In these configurations, the nitrogen-to-nitrogen distance of the CN⁻ ligand to Lys563 is significantly increased to 3.8 – 3.9 Å, whereas that to His93 is nearly unchanged. The corresponding calculated stretching frequencies are now much closer to the experimental value (Table 2).

The two optimised active site structures with the more tilted CN⁻ geometries exhibited an open space, which allowed binding of an OH⁻ to Fe₁. To assess the influence of such a

ligand on the C≡N stretching frequency and to get an equivalent structure of the CN⁻ inhibited state observed in CODH_{Mt} (pdb: 3I04)⁷, an OH⁻ ligand was introduced. In these structures (CODHII_{Ch}-CN/tilt/OH⁻; CODHII_{Ch}-C_{red1}-CN/tilt/OH⁻), geometry optimizations caused the tilt angle to increase from ~18° to ~35° because of increased steric interactions, consistent with the experimentally determined tilt angle in CODH_{Mt} (~30°). In addition to the hydrogen bond formed with the Nε of His93, the hydroxyl ligand also provides an extra hydrogen bond to the CN⁻ molecule thereby contributing to a significant decrease of the stretching frequency down to 2054 cm⁻¹ (Table 2).

Whereas in all geometries, His93 remains in H-bond distance, the tilt angle geometry seems to depend on the interactions of the CN⁻ ligand with Lys593. To assess the role of Lys593, we have generated the CODHII_{Ch}-CN/K563A structure *in silico*, starting from that of the wild-type protein complex (pdb: 5FLE). Optimization leads to a tilt angle of ca. 24° and the resultant calculated C≡N stretching frequency (2112 cm⁻¹) agrees well with the experimental frequency of 2102 cm⁻¹ (Table 2).

Additional information about the potential interactions of Lys593 with the cyanide ligand was provided by the optimised CODHII_{Ch}-CN (wild-type) structure including a deprotonated Lys593 side chain. Also in this case, calculated (2109 cm⁻¹) and experimental (2110 cm⁻¹) C≡N stretching frequencies nearly coincide (Table 2).

Discussion

Cyanide-inhibition of Ni-dependent CODHs has been investigated for many years using a variety of experimental approaches. The analysis of the CODH-CN complex is thought to contribute to a better understanding of the catalytic mechanism but, the previous studies did not yet provide a consistent view about the structure of the cyanide-bound active site and its degradation pathway.

The cyanide binding site:

Early IR spectroscopic studies revealed two different C≡N stretching modes that, due to their dependence on the cyanide concentration, were interpreted in terms of different modes of cyanide binding. Although the previously proposed bridging position between Fe₁ and Ni has been meanwhile discarded, the view of two different binding geometries was re-animated on the background of slightly different active geometries derived from X-ray crystallography⁷⁻⁸. In an attempt to reconcile crystallographic⁷⁻⁸ and spectroscopic data (ENDOR, Mössbauer)³⁸⁻³⁹, a two-step inhibition mechanism was proposed³⁶. In the first step, CN⁻ was suggested to bind reversibly to Ni in a distorted tetrahedral geometry of the coordinated Ni ion as suggested by the crystal structure of CODH_{Mt}. This step may be similar to CO binding whereas in the second step, the release of a OH⁻ ligand of Fe₁, previously suggested to bind to C_{red1}³⁸, is followed by a slow reorganization of the cofactor that allows CN⁻ to bind more

tightly to the C-cluster. This is thought to be reflected by the square planar coordination geometry of Ni observed in CODHII_{Ch}. The different CN⁻ concentrations used for inhibition of both the CODHII_{Ch} and CODH_{Mt} crystals in soaking solutions were suggested to be the origin of these two binding modes.

In the present work, we have now shown that the previously reported frequencies of 2037 and 2079 cm⁻¹ do not refer to the cyanide bound to the cofactor but originate from free CN⁻ (2080 cm⁻¹) and the degradation product [Fe(CN)₆]⁴⁻ (2037 cm⁻¹). Instead, the intact cofactor-CN adduct gives rise to a band at 2110 cm⁻¹. This band is observed at the same position for the enzyme in solution and in the crystalline state. Accordingly, the IR spectroscopic data should originate from the same state to which the crystallographic model refers to and which served as the starting point for the theoretical approaches. Specifically, QM/MM calculations indicate that the cofactor-CN adduct is characterised by the lack of an OH⁻ ligand at the Fe₁ as the hydrogen bonding interactions would cause a substantial downshift of this mode by ca. 50 cm⁻¹ compared to the experimental value (2110 cm⁻¹). A band at such a low frequency that could be ascribed to a Fe₁(OH⁻)Ni(CN⁻) adduct is not observed at any experimental condition employed in this work. This negative result does not *per se* rule out the existence of such an intermediate state. However, if it exists, it is not accumulated even at sub-stoichiometric CODHII_{Ch}/CN⁻ ratios and must, instead, decay quite rapidly on the sub-minute time scale to the stable Fe₁Ni(CN) adduct.

Mechanism of the cyanide inhibition and degradation of the C-cluster:

Once the CODHII_{Ch}-CN complex was formed according to protocol A, i.e. after removal of excess cyanide, it remained stable for hours at 10°C but the cyanide ligand can be removed at elevated temperature in the presence of CO, accompanied with a recovery of the enzymatic activity. Conversely, a large excess of cyanide accelerates the degradation of the cofactor that is observed on the time scale of hours and eventually leads to the formation of the stable [Fe(CN)₆]⁴⁻ and [Ni(CN)₄]²⁻ complexes. These findings point to a two-step inhibition mechanism. First, cyanide rapidly binds to the Ni ion and induces the release of the OH⁻ ligand from Fe₁. This process can be reversed at high temperature in the presence of CO. In the second step, an additional cyanide binds to Fe₁, albeit with a much slower rate, such that this step and thus the irreversible degradation can be efficiently blocked upon removal of excess cyanide after CN⁻ binding to Ni (protocol A). Since the IR spectra provide no indication for a C-cluster coordinated by two cyanides, CN⁻ binding to Fe₁ appears to be followed by the rapid decomposition of the cofactor into the [Fe(CN)₆]⁴⁻ and [Ni(CN)₄]²⁻ complexes.

Structure of the CN⁻-cofactor adduct:

As already shown in previous studies on hydrogenases, the stretching frequency of the metal-bound cyanide ligand depends sensitively on the geometry of the cofactor, its

electronic configuration, as well as on the electrostatics in the binding pocket, including hydrogen bonding interactions⁴⁰⁻⁴¹. To assess the importance of these parameters and to relate the observed frequency with the crystallographic data, we have employed QM/MM calculations. Starting with the coordinates of the high-resolution structural model determined in this work, the QM/MM-optimised cofactor structure displays a very good agreement but the corresponding C≡N stretching frequency is distinctly underestimated by 36 cm⁻¹. This deviation is much larger than the inherent inaccuracy of the theoretical approach (Table S2 of ESI). In contrast, a good frequency match was obtained for the optimised structure of the Lys563A variant in which the positively charged side chain in the vicinity of the cyanide ligand is removed. Furthermore, the optimised geometry of the C-cluster displays a large tilt angle (ca. 24°) which is also obtained upon optimizing the high-resolution wild-type structure but using a deprotonated Lys563. Here the increase of the tilt angle is accompanied by an increased nitrogen-nitrogen distance of the cyanide ligand to the Lys563 from 3 to 4 Å, suggesting a substantial weakening of the (electrostatic) interactions with the cyanide ligand. Also in this case, the calculated frequency agrees very well with the experimental value. The same large nitrogen-nitrogen distance but a somewhat smaller tilt angle is obtained for the wild-type protein upon raising the initial value for the tilt angle prior to optimization. Again, an excellent agreement with the experimental C≡N stretching frequency was obtained. In all optimised structures, the N_ε atom of His93 remains at a distance of 2.7 Å which, together with the nearly linear (Ni)CN-H-N_ε(His93) geometry, points to strong hydrogen bonding interactions. Conversely, the comparison of calculated and experimental C≡N stretching frequencies indicates that the interactions between the cyanide ligand and Lys563 must be weak, corresponding to a relatively large nitrogen-to-nitrogen distance (4 Å). Such weak interactions point to a deprotonated side chain of Lys563. The potential proton acceptor is readily identified as the hydroxyl ligand of Fe₁ which is released upon cyanide binding to the Ni. Furthermore, the time-independent frequency and intensity of the C≡N stretching indicates that Lys563 remains deprotonated over the time scale of hours, implying that the active site of the cyanide-bound C_{red1} state is not accessible for protons from the solution side via the proton channel identified in CODH_{Mt}²⁰.

It might be that structural changes along the proton channel in the cyanide-bound complex may impair reprotonation of Lys563. However, the present structure of the cyanide-complex does not permit an unambiguous conclusion (*vide infra*). As an alternative interpretation, one may invoke a redox-state dependent proton transfer. This view is consistent with the high turnover number for CO oxidation at the C_{red1} state which requires a rapid *and* unidirectional proton translocation from the C-cluster to the solution. The reverse proton translocation occurs during enzymatic CO₂ reduction which, in turn, is based on the C_{red2} state. Accordingly, the oxidation state of the C-cluster controls the

directionality of the proton transfer such that reprotonation of Lys563 is inhibited in the cyanide complex of C_{red1}.

A deprotonated Lys563, however, is not consistent with the present high-resolution structure of the CODHII_{Ch}-CN complex which displays a distance of only 3 Å, concomitant to a smaller tilt angle, and thus points to appreciable Lys563-cyanide interactions. Whereas X-ray crystallography reflects the protein including a protonated side chain, the IR spectra that are identical in the crystalline state at low temperature and in solution at ambient temperature indicate a deprotonated Lys563 residue. To reconcile these findings, we suggest that, during accumulation of the diffraction data, radiation damage at the C-cluster may cause generation of a hydroxyl radical from a water molecule in the vicinity of Lys563, which is associated with a distinctly lower pK_a of ca. 11.⁴² As a consequence, protonation of the Lys side chain could occur.

Conclusions

In the present study we have unambiguously identified the C≡N stretching mode of the cyanide bound complex of CODHII_{Ch}, confirming that a single cyanide is bound to the Ni ion. Additional IR bands observed in previous investigations could be attributed to free cyanide or to degradation products of the C-cluster. This complete cyanide-induced degradation of the Fe-Ni center only occurs in the presence of excess cyanide. In the absence of excess cyanide, the CODHII_{Ch}-CN complex is stable for hours at ambient temperature and enzymatic activity towards CO oxidation can even be recovered at elevated temperature. On the basis of QM/MM calculations the CODHII_{Ch}-CN complex, cyanide binding to the Ni occurs upon release of the hydroxyl ligand from the Fe. The hydroxyl ligand captures a proton from the side chain of Lys563. On the other hand, the present crystallographic data point to a protonated Lys563, which is not compatible with the IR spectroscopic data obtained from CODHII_{Ch}-CN crystals. This discrepancy is suggested to be due to reprotonation of Lys563 via a water radical, generated *in situ* upon X-ray irradiation. The IR spectroscopic data, however, indicate that in the cyanide complex Lys563 remains deprotonated for hours. This finding prompted us to suggest a redox-state dependent directionality of proton translocation through the proton channel connecting the solution phase with the active site. This interpretation is consistent with the enzymatic processes that require proton release from and proton uptake by the active site in the C_{red1} state (CO oxidation) and C_{red2} state (CO₂ reduction), respectively.

The present results and the proposed interpretations demand for further experimental and theoretical investigations of the proton translocation mechanisms and the protonation pattern of the different active site states during the enzymatic reaction sequences.

Acknowledgements

This research has been financed by the Deutsche Forschungsgemeinschaft, Cluster of Excellence "Unicat".

The authors thank the Alexander-von-Humboldt Foundation (to Alexandre Ciaccafava) and the Federation of European Biochemical Societies (to Alexandre Ciaccafava) for financial support.

References:

1. A. M. Appel, J. E. Bercaw, A. B. Bocarsly, H. Dobbek, D. L. DuBois, M. Dupuis, J. G. Ferry, E. Fujita, R. Hille, P. J. A. Kenis, C. A. Kerfeld, R. H. Morris, C. H. F. Peden, A. R. Portis, S. W. Ragsdale, T. B. Rauchfuss, J. N. H. Reek, L. C. Seefeldt, R. K. Thauer and G. L. Waldrop, *Chem. Rev.*, 2013, **113**, 6621-6658.
2. J. H. Jeoung and H. Dobbek, *Science*, 2007, **318**, 1461-1464.
3. J. Heo, C. R. Staples, C. M. Halbleib and P. W. Ludden, *Biochemistry*, 2000, **39**, 7956-7963.
4. V. Svetlitchnyi, C. Peschel, G. Acker and O. Meyer, *J. Bacteriol.*, 2001, **183**, 5134-5144.
5. S. A. Ensign, *Biochemistry*, 1995, **34**, 5372-5381.
6. J. H. Jeoung and H. Dobbek, *J. Biol. Inorg. Chem.*, 2011, **17**, 167-173.
7. Y. Kung, T. I. Doukov, J. Seravalli, S. W. Ragsdale and C. L. Drennan, *Biochemistry*, 2009, **48**, 7432-7440.
8. J. H. Jeoung and H. Dobbek, *J. Am. Chem. Soc.*, 2009, **131**, 9922-9923.
9. J. Fessler, J.-H. Jeoung and H. Dobbek, *Angew. Chem. Int. Ed.*, 2015, **54**, 8560-8564.
10. W. Gong, B. Hao, Z. Wei, D. J. Ferguson, T. Tallant, J. A. Krzycki and M. K. Chan, *Proc. Natl. Acad. Sci.*, 2008, **105**, 9558-9563.
11. P. Amara, J. M. Mouesca, A. Volbeda and J. C. Fontecilla-Camps, *Inorg. Chem.*, 2011, **50**, 1868-1878.
12. D. Qiu, M. Kumar, S. W. Ragsdale and T. G. Spiro, *J. Am. Chem. Soc.*, 1997, **119**, 11134-11134.
13. D. Qiu, M. Kumar, S. W. Ragsdale and T. G. Spiro, *J. Am. Chem. Soc.*, 1996, **118**, 10429-10435.
14. U. Mueller, N. Darowski, M. R. Fuchs, R. Forster, M. Hellmig, K. S. Paithankar, S. Puhlinger, M. Steffien, G. Zocher and M. S. Weiss, *J. Synchrotron Radiat.*, 2012, **19**, 442-449.
15. M. Krug, M. S. Weiss, U. Heinemann and U. Mueller, *J. Appl. Crystallogr.*, 2012, **45**, 568-572.
16. P. D. Adams, P. V. Afonine, G. Bunkoczi, V. B. Chen, I. W. Davis, N. Echols, J. J. Headd, L.-W. Hung, G. J. Kapral, R. W. Grosse-Kunstleve, A. J. McCoy, N. W. Moriarty, R. Oeffner, R. J. Read, D. C. Richardson, J. S. Richardson, T. C. Terwilliger and P. H. Zwart, *Acta Crystallogr. Sect. D*, 2010, **66**, 213-221.
17. P. Emsley, B. Lohkamp, W. G. Scott and K. Cowtan, *Acta Crystallographica Section D*, 2010, **66**, 486-501.
18. G. N. Murshudov, P. Skubak, A. A. Lebedev, N. S. Pannu, R. A. Steiner, R. A. Nicholls, M. D. Winn, F. Long and A. A. Vagin, *Acta Crystallogr. Sect. D*, 2011, **67**, 355-367.
19. M. D. Winn, C. C. Ballard, K. D. Cowtan, E. J. Dodson, P. Emsley, P. R. Evans, R. M. Keegan, E. B. Krissinel, A. G. W. Leslie, A. McCoy, S. J. McNicholas, G. N. Murshudov, N. S. Pannu, E. A. Potterton, H. R. Powell, R. J. Read, A. Vagin and K. S. Wilson, *Acta Crystallogr. Sect. D*, 2011, **67**, 235-242.
20. E. J. Kim, J. Feng, M. R. Bramlett and P. A. Lindahl, *Biochemistry*, 2004, **43**, 5728-5734.
21. J. C. Phillips, R. Braun, W. Wang, J. Gumbart, E. Tajkhorshid, E. Villa, C. Chipot, R. D. Skeel, L. Kalé and K. Schulten, *J. Comput. Chem.*, 2005, **26**, 1781-1802.
22. A. D. MacKerell, D. Bashford, M. Bellott, R. L. Dunbrack, J. D. Evanseck, M. J. Field, S. Fischer, J. Gao, H. Guo, S. Ha, D. Joseph-McCarthy, L. Kuchnir, K. Kuczera, F. T. K. Lau, C. Mattos, S. Michnick, T. Ngo, D. T. Nguyen, B. Prodhom, W. E. Reiher, B. Roux, M. Schlenkrich, J. C. Smith, R. Stote, J. Straub, M. Watanabe, J. Wiórkiewicz-Kuczera, D. Yin and M. Karplus, *J. Phys. Chem. B*, 1998, **102**, 3586-3616.
23. A. K. Rappe, C. J. Casewit, K. S. Colwell, W. A. Goddard and W. M. Skiff, *J. Am. Chem. Soc.*, 1992, **114**, 10024-10035.
24. P. Sherwood, A. H. de Vries, M. F. Guest, G. Schreckenbach, C. R. A. Catlow, S. A. French, A. A. Sokol, S. T. Bromley, W. Thiel, A. J. Turner, S. Billeter, F. Terstegen, S. Thiel, J. Kendrick, S. C. Rogers, J. Casci, M. Watson, F. King, E. Karlsen, M. Sjøvoll, A. Fahmi, A. Schäfer and C. Lennartz, *J. Mol. Struct. THEOCHEM*, 2003, **632**, 1-28.
25. A. D. Becke, *Phys. Rev. A*, 1988, **38**, 3098-3100.
26. L. Yu, C. Greco, M. Bruschi, U. Ryde, L. De Gioia and M. Reiher, *Inorg. Chem.*, 2011, **50**, 3888-3900.
27. S. R. Billeter, A. J. Turner and W. Thiel, *Phys. Chem. Chem. Phys.*, 2000, **2**, 2177-2186.
28. M. J. Frisch, G. W. Trucks, H. B. Schlegel, G. E. Scuseria, M. A. Robb, J. R. Cheeseman, G. Scalmani, V. Barone, B. Mennucci, G. A. Petersson, H. Nakatsuji, M. Caricato, X. Li, H. P. Hratchian, A. F. Izmaylov, J. Bloino, G. Zheng, J. L. Sonnenberg, M. Hada, M. Ehara, K. Toyota, R. Fukuda, J. Hasegawa, M. Ishida, T. Nakajima, Y. Honda, O. Kitao, H. Nakai, T. Vreven, J. A. Montgomery Jr., J. E. Peralta, F. Ogliaro, M. J. Bearpark, J. Heyd, E. N. Brothers, K. N. Kudin, V. N. Staroverov, R. Kobayashi, J. Normand, K. Raghavachari, A. P. Rendell, J. C. Burant, S. S. Iyengar, J. Tomasi, M. Cossi, N. Rega, N. J. Millam, M. Klene, J. E. Knox, J. B. Cross, V. Bakken, C. Adamo, J. Jaramillo, R. Gomperts, R. E. Stratmann, O. Yazyev, A. J. Austin, R. Cammi, C. Pomelli, J. W. Ochterski, R. L. Martin, K. Morokuma, V. G. Zakrzewski, G. A. Voth, P. Salvador, J. J. Dannenberg, S. Dapprich, A. D. Daniels, Ö. Farkas, J. B. Foresman, J. V. Ortiz, J. Cioslowski and D. J. Fox, *Gaussian, Inc., Wallingford CT*, 2009.
29. K. Nakamoto, *Infrared and Raman Spectra of Inorganic and Coordination Compounds*, Wiley, Hoboken, N.J., 2009.
30. S. Yoshikawa, D. H. O'Keeffe and W. S. Caughey, *J. Biol. Chem.*, 1985, **260**, 3518-3528.
31. K. S. Reddy, T. Yonetani, A. Tsuneshige, B. Chance, B. Kushkuley, S. S. Stavrov and J. M. Vanderkooi, *Biochemistry*, 1996, **35**, 5562-5570.
32. S. W. Ha, M. Korbas, M. Klepsch, W. Meyer-Klaucke, O. Meyer and V. Svetlitchnyi, *J. Biol. Chem.*, 2007, **282**, 10639-10646.
33. S. Kim, D. C. Sorescu and J. T. Yates, *J. Phys. Chem. C*, 2007, **111**, 5416-5425.
34. P. Yu, F. Yang, J. Zhao and J. Wang, *J. Phys. Chem. B*, 2014, **118**, 3104-3114.
35. G. M. Sando, Q. Zhong and J. C. Owrutsky, *J. Chem. Phys.*, 2004, **121**, 2158-2168.
36. Y. Kung and C. L. Drennan, *Curr. Opin. Chem. Biol.*, 2011, **15**, 276-283.
37. M. Can, F. A. Armstrong and S. W. Ragsdale, *Chem. Rev.*, 2014, **114**, 4149-4174.
38. V. J. DeRose, J. Telsler, M. E. Anderson, P. A. Lindahl and B. M. Hoffman, *J. Am. Chem. Soc.*, 1998, **120**, 8767-8776.

39. Z. G. Hu, N. J. Spangler, M. E. Anderson, J. Q. Xia, P. W. Ludden, P. A. Lindahl and E. Munch, *J. Am. Chem. Soc.*, 1996, **118**, 830-845.

40. M. Horch, Y. Rippers, M. A. Mroginski, P. Hildebrandt and I. Zebger, *Chemphyschem*, 2013, **14**, 185-191.

41. Y. Rippers, M. Horch, P. Hildebrandt, I. Zebger and M. A. Mroginski, *Chemphyschem*, 2012, **13**, 3852-3856.

42. G. A. Poskrebyshv, P. Neta and R. E. Huie, *J. Phys. Chem. A*, 2002, **106**, 11488-11491.